2015 International Nuclear Atlantic Conference - INAC 2015
São Paulo, SP, Brazil, October 4-9, 2015
ASSOCIAÇÃO BRASILEIRA DE ENERGIA NUCLEAR - ABEN
ISBN: **978-85-99141-06-9**

CFD-DEM SIMULATION OF A CONCEPTUAL GAS-COOLED FLUIDIZED BED NUCLEAR REACTOR

Lucilla C. Almeida[1,2], João Aguirre[2] and Jian Su[1]

[1] Nuclear Engineering Program, COPPE
Universidade do Federal do Rio de Janeiro
21941-972, Rio de Janeiro - RJ - Brasil
lucillalmeida@gmail.com
sujian@nuclear.ufrj.br

[2] Engineering Simulation and Scientific Software, ESSS
Av. Presidente Vargas, 3131
20210-031, Rio de Janeiro - RJ - Brasil
aguirre@rocky-dem.com

ABSTRACT

Several conceptual designs of the fluidized-bed nuclear reactor have been proposed due to its many advantages over conventional nuclear reactors such as PWRs and BWRs. Amongst their characteristics, the enhanced heat transfer and mixing enables a more uniform temperature distribution, reducing the risk of hot-spot and excessive fuel temperature, in addition to resulting in a higher burnup of the fuel. Furthermore, the relationship between the bed height and reactor neutronics turns the coolant flow rate control into a power production mechanism. Moreover, the possibility of removing the fuel by gravity from the movable core in case of a loss-of-cooling accident increases its safety. High-accuracy modeling of particles and coolant flow in fluidized bed reactors is needed to evaluate reliably the thermal-hydraulic efficiency and safety margin. The two-way coupling between solid and fluid can account for high-fidelity solid-solid interaction and reasonable accuracy in fluid calculation and fluid-solid interaction. In the CFD-DEM model, the particles are modeled as a discrete phase, following the DEM approach, whereas the fluid flow is treated as a continuous phase, described by the averaged Navier-Stokes equations on a computational cell scale. In this work, the coupling methodology between Fluent and Rocky is described. The numerical approach was applied to the simulation of a bubbling fluidized bed and the results were compared to experimental data and showed good agreement.

1. INTRODUCTION

Fluidized beds are widely used in many plant operations in chemical, energy production, oil and gas, mineral and agricultural industries, mainly due to their good mixing characteristics and high contact surface area between gas and solid phases. Various designs of the fluidized-bed nuclear reactor concept have been studied and their feasibility demonstrated [1, 2, 3]. In general, a fluidized bed nuclear reactor consists of a graphite-walled tube partially filled with coated fuel particles. In contrast with other HTGRs where the fuel is encased as a graphite pebble or rods, the particles are arranged in the bottom part of the cavity, forming a packed bed. The coolant flows from bottom to top through the tube, thereby fluidizing the particle bed [3]. Figure 1 shows a schematic view of a fluidized bed reactor in a packed bed (left) and in a fluidized state (right).

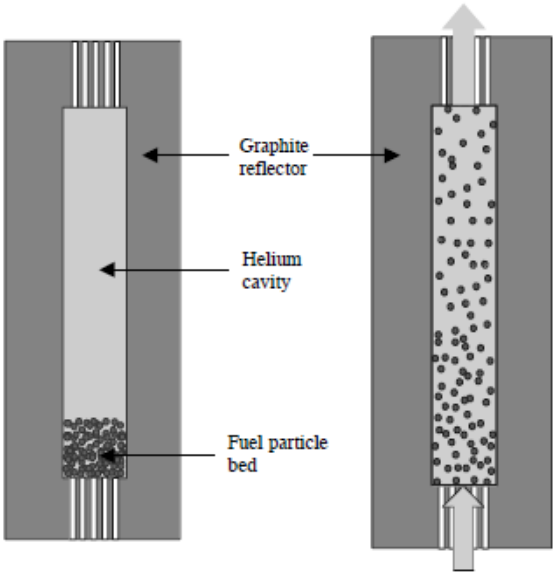

Figure 1: Schematic view of a fluidized bed reactor at packed condition (left) and at fluidized state (right).

The fluidized bed concept has many advantages for a nuclear reactor. In addition to the high heat transfer rates between fluid and particles possible with this type, the intimate mixing and agitation result in a uniform temperature distribution throughout the bed, reducing the hot-spot factor and yielding a high temperature of fluid without leading to an excessive fuel temperature. For the same reasons, there results an even, and consequently high, burnup of all the fuel, irrespective of the shape of the neutron-flux distribution [2, 3].

Furthermore, the bed height increases as the gas flow rate increases, and this change of the bed geometry affects the reactor neutronics, consequently the power production can be controlled by the inlet flow rate, reducing the dependency on other control mechanisms. The static and dynamic behavior of enriched uranium oxide fuel in a simple reactor geometry has been analyzed and its advantages presented, for example in [4, 5, 3].

Besides that, the appeal of the movable core lies in the possibility of having an additional degree of freedom to improve reactor safety, since after a possible loss-of-coolant accident, (LOCA), the fuel may be removed by gravity to a passively cooled storage place outside the core[6]. It also has the characteristics of being simple in design, therefore cheaper and modular in system, hence any reactor size can be constructed from the basic standard module.

Despite their widespread application, much of the development and design of fluidized bed reactors has been empirical as the complex flow behavior of gas–solid flow in these systems makes flow modeling a challenging task [7]. With the increase on computational capacity, numerical simulation methods have been increase held as suitable to provide complete information of granular flows [8]. The coupled DEM-CFD approach is a promising alternative for modelling granular-fluid systems, introduced by early developers [9, 10, 11]. In the CFD-DEM model, the particles are modeled as a discrete phase, following the DEM approach, whereas the fluid flow is treated as a continuous phase, described by the averaged Navier-Stokes equations on a computational cell scale [12]. This approach has been recognized as an effective method to study particle–fluid flows [13].

In this work, coupling between DEM package Rocky® and CFD package Fluent® will be demonstrated. Rocky® is a powerful DEM software, capable of performing 3D simulations of granular flows. It uses real particle geometries and deals with 3D surface wear modification, particle breakage, sticky particles as well as rotating and vibrating boundaries. Fluent® package is well established as one of the world leaders for CFD applications. The proposed approach was applied to the simulation of a bubbling fluidized bed, based on case 1 of the 2013 NETL small scale challenge problem (SSCP-I) [14]. The numerical results were compared to experimental data and showed good agreement.

2. MODEL DESCRIPTION

This section will provide a brief description of DEM, CFD and coupling methods.

2.1. Discrete Element Method

Granular material flows are very difficult to handle numerically as they can behave both similar to solid (for example when pile of sand sits on a surface) or as a fluid (for example when this sand is falling from some height). This type of behavior creates substantial difficulties for the derivation of the general-case equations of motion and equation of state for a granular media.

The Discrete Element Method is a numerical technique that avoids this problem via "brute force" approach, i.e. by simulation of the motion of every particle in a granular matter. Instead of numerical integration of the continuum equations of motion and state, the equations of motion of every single particle are numerically integrated.

In the frame of the DEM, all particles within the computational domain are tracked in a Lagrangian way, by solving explicitly Newton's second law that governs translational (Equation (1)) and rotational particle motion (Equation (2)):

$$m_p \frac{d\mathbf{v}}{dt} = \mathbf{F}_p^C + \mathbf{F}_p^{F\to p} + m_p\mathbf{g} \tag{1}$$

$$\mathbf{I}_p \frac{d\boldsymbol{\omega}_p}{dt} = \mathbf{T}_p \tag{2}$$

where $\mathbf{v}$ is the particle velocity vector, m_p is the particle mass, $\mathbf{g}$ is the gravitational acceleration vector, $\mathbf{F}_p^{\mathrm{C}}$ is the contact force that accounts for particle-particle and particle-wall interactions, ω_p is the angular velocity vector, $\mathbf{T}_p$ is the net torque generated by tangential forces that causes the rotation of the particle and $\mathbf{I}_p$ is its moment of inertia. An additional force, $\mathbf{F}_p^{\mathrm{F}\to p}$, accounts for fluid-particle interaction by summing all fluid forces acting on the particle, which will be explained later.

In general, contact forces can be decomposed in two orthogonal components, consisting of normal forces, $\mathbf{F}_{n,p}$, and tangential forces $\mathbf{F}_{t,p}$, with respect to the contact plane, as can be seen in Equation (3).

$$\mathbf{F}_p^C = \mathbf{F}_{n,p} + \mathbf{F}_{t,p} \tag{3}$$

In Rocky®, particles are allowed to slightly overlap, as illustrated by Figure 2 and the contact forces are calculated based on values of this overlap. Normal and tangential directions are defined as a function of normal overlap and tangential relative particle displacement as seen in the models described in the following sections.

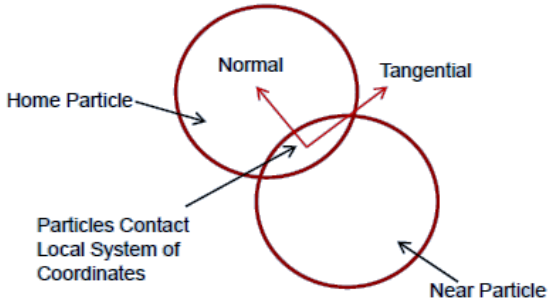

Figure 2: Particle contact force with overlapping particles.

2.1.1. Normal Contact Forces

Linear hysteresis is an elastic-plastic model that allows the simulation of the plastic energy dissipation on a contact with the advantage of not incurring in large simulation times. Other advantages are that the contact energy dissipation is not sensitive to other simultaneous contacts, the force is zero at zero contact deformation as expected, the energy dissipation does not depend on loading rate and the coefficient of restitution is velocity independent [15]. On the other hand, contact force and overlap history has to be retained, which makes it more difficult to implement.

In this model, the shape of overlap-normal force is approximated with two straight lines of different slopes, one for loading and other for unloading, as illustrated on Figure 3 for a collision of a 100 mm particle on a flat plate. These forces are calculated in Rocky by the equations set composed by Equation (4), Equation (5) and Equation (6). More detailed information can be found in [15].

$$\mathbf{F}_{n,p}^t = \min\left(\mathbf{F}_{n,p}^{t-dt} + K_{nu} ds_n, K_{nl} s_n\right) \text{ if } ds_n \geq 0 \tag{4}$$

$$\mathbf{F}_{n,p}^t = \max\left(\mathbf{F}_{n,p}^{t-dt} + K_{nu} ds_n, 0.001 K_{nl} s_n\right) \text{ if } ds_n < 0 \tag{5}$$

$$ds_n = s_n^t - s_n^{t-dt} \tag{6}$$

where $\mathbf{F}_{n,p}{}^t$ is the normal elastic-plastic contact force at the current time step, $\mathbf{F}_{n,p}{}^{t\text{-}dt}$ is the same force at the previous time step. ds_n is the change in the contact normal overlap during time step and is assumed to be positive as particles approach each other and negative when they separate, $s_n{}^t$ and $s_n{}^{t\text{-}dt}$ are the normal overlap value at current and previous time step.

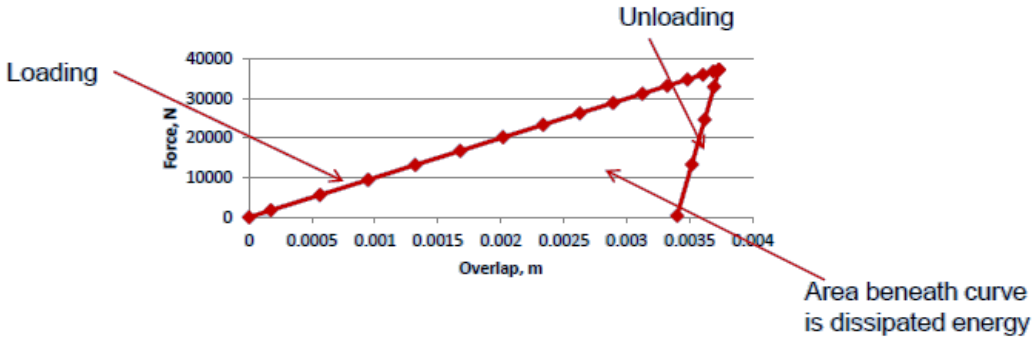

Figure 3: Normal force from Rocky simulation at a collision of 100 mm particle on a flat plate.

In the contact force equations, K_{nl} and K_{nu} are the values of the contact stiffness for loading and unloading parts. More details of their computation based on the particle and boundary material stiffnesses and particle size can be found at [16]. This model is appropriate for flow of non-adhesive materials. For cases involving adhesive materials, other models implemented in Rocky® are more suitable.

2.1.2. Tangential contact forces

The linear elastic-frictional model is used. This model has simple elastic behavior before onset of friction, which is on the majority of DEM codes relies on, and can reproduce Coulomb frictional contact behavior for static and dynamic frictional values. However, contact force and displacement history has to be retained, which makes this model more difficult to implement.

If no sliding is taking place for the contact, the Equation (7) is considered for the tangential force computation:

$$\mathbf{F}_{t,p}^{t} = \min\left(\mathbf{F}_{t,p}^{t-dt} + K_{nl} ds_t, \mu_s \mathbf{F}_{n,p}^{t}\right) \tag{7}$$

If sliding is taking place for the contact, then the Equation (8) is used:

$$\mathbf{F}_{t,p}^{t} = \min\left(\mathbf{F}_{t,p}^{t-dt} + K_{nl} ds_t, \mu_d \mathbf{F}_{n,p}^{t}\right) \tag{8}$$

Where $\mathbf{F}_{t,p}{}^{t}$ is the tangential contact force at the current time step, $\mathbf{F}_{t,p}{}^{t\text{-}dt}$ is the same force at the previous time step, ds_t is tangential relative particles displacement during time step, μ_s and μ_d are static and dynamic friction coefficients. The sliding is considered to be taking place on the contact when tangential force exceeds the limit of $\mu_s \mathbf{F}^{t}_{n}$. Once tangential force falls below the value of $\mu_d \mathbf{F}^{t}_{n}$, the contact is considered non-sliding again.

2.2. CFD Approach

A large number of researchers carried studies to achieve basic understanding of the complex flows involving multiphase systems during past years. Basic equations are usually formulated using volume or ensemble averaging methods [17]. Derivation of basic multiphase flow equations and different averaging methods can be found in [12, 18, 19, 20]. In this work, the

classical Navier-Stokes equations are modified and averaged in volume [12], returning the same expressions obtained with the TFM equations unless only one phase is considered [21]. This enabled the usage of Fluent® solver in this coupling implementation with Rocky®.

The averaged mass and momentum conservation equations are written as:

$$\frac{\partial}{\partial t}\left(\alpha_f \rho_f\right) + \nabla \cdot \left(\alpha_f \rho_f \mathbf{u}\right) = 0 \tag{9}$$

$$\frac{\partial}{\partial t}\left(\alpha_f \rho_f \mathbf{u}\right) + \nabla \cdot \left(\alpha_f \rho_f \mathbf{u}\mathbf{u}\right) = -\alpha_f \nabla P + \alpha_f \nabla \cdot \tau_f + \alpha_f \rho_f \mathbf{g} - \mathbf{F}^{p \to F} \tag{10}$$

where $\mathbf{u}$ is the fluid velocity, τ_f is the viscous stress tensor of the gas phase, α_f stands for the fluid volume fraction, P is the pressure, and ρ_f is the fluid density.

To solve this set of equations, the commercial code Fluent® was used, which uses the finite volume method, cell centered and uses an implicit scheme for time stepping. A block algebraic multigrid solver is used for the solution of the linearized equations [22]. The secondary phase momentum equations are not solved by Fluent®, as the dispersed phase velocity comes from the DEM solver. A source term is included on the disperse phase continuity equation to impose the disperse volume fraction calculated at the DEM side. The momentum exchange term is not calculated in the CFD solver, but on the DEM side, as explained in the next section, and included in the formulation through a source term in the continuous phase momentum equation. The PC-SIMPLE algorithm, which is the SIMPLE algorithm extended to multiphase flows, was used for the pressure-velocity coupling. More detailed information about this coupling segregated pressure-based method can be found at [17].

2.3. Interphase Coupling

The influence of the fluid flow on the particle motion is achieved by the term $\mathbf{F}_p^{\mathrm{F}\to p}$ in Equation (1). This term sums all the fluid forces acting on the particle, amongst which the main are the drag force and pressure gradient force, as well as non-drag forces such as virtual mass, Basset force, Saffman lift (due to velocity gradients) and Magnus lift (due to particle rotation) forces, etc. Depending on the flow conditions, most of these forces can be neglected. In this study, only the drag force, $\mathbf{F}_D$, and the pressure gradient force, $\mathbf{F}_{\nabla P}$, were considered.

The pressure gradient force is given by:

$$\mathbf{F}_{\nabla P} = -V_p \nabla P \tag{11}$$

where V_p is the volume of the particle and P is the pressure at particle location. The drag force is calculated as:

$$\mathbf{F}_D = \beta\left(\mathbf{u} - \mathbf{v}\right) \tag{12}$$

where β is the momentum transfer coefficient. The drag force exerted on a single particle is different from the drag force on a particle surrounded by other particles. Therefore, the

coefficient β depends on the volume fraction of the cell where the drag is computed as well as the drag coefficient, as can be seen in Equation **(13)**.

$$\beta = \frac{3}{4}\frac{(1-\alpha_f)\rho_f C_D}{d_p}|\mathbf{v}-\mathbf{u}| \tag{13}$$

For a relatively low particle concentration (α_p < 0.2), Wen & Yu developed a drag law correlation based on a series of experiments on fluidized beds [20]. This correlation is presented in terms of a correction (based on α_f) of the Schiller & Naumann correlation. To higher solids volume fractions, the Wen & Yu drag law deviates from the experimental data. For these cases, with solids volume fraction α_p < 0.2 up to maximum packing limit, Ergun has developed a correlation to the head loss in fixed beds [23].

To make the transition between the Wen & Yu and Ergun correlations in a smooth way, Huilin & Guidaspow have applied a blending function to promote the link based on the fluid volume fraction. The final drag correlation used in this work is given by Equation **(14)**.

$$C_{D,Huilin\&Guidaspow} = \psi C_{D,Ergun} + (1-\psi) C_{D,Wen\&Yu} \tag{14}$$

$$C_{D,Wen\&Yu} = \begin{cases} \dfrac{24}{\alpha_f \,\mathrm{Re}}\left[1+0.15(\alpha_f\,\mathrm{Re})^{0.687}\right]\alpha_f^{-1.65} & \alpha_f\,\mathrm{Re} < 1000 \\ 0.44\alpha_f^{-1.65} & \alpha_f\,\mathrm{Re} < 1000 \end{cases} \tag{15}$$

$$C_{D,Ergun} = 200\frac{(1-\alpha_f)}{\alpha_f \phi^2\,\mathrm{Re}} + \frac{7}{3\phi} \tag{16}$$

where the blending function ψ is defined as:

$$\psi = \frac{\arctan\left(150\cdot 1.75(0.8-\alpha_f)\right)}{\pi} + 0.5 \tag{17}$$

and Re is the relative particle Reynolds number, defined using the particle diameter and the relative particle-fluid velocity in Equation (18).

$$\mathrm{Re} = \frac{\rho_f |\mathbf{v}-\mathbf{u}| d_p}{\mu_f} \tag{18}$$

The influence of the particles on the fluid flow is taken into account not only by the volume fraction in the VANS equations, but also by the force $\mathbf{F}^{p\to F}$ in Equation (10). A semi-implicit treatment of the reactive force is adopted and the momentum exchange with the particulate phase is calculated as:

$$\mathbf{F}^{p\to F} = \frac{\sum_{p=1}^{N} \mathbf{F}_p^{F\to p}}{V_{cell}} \tag{19}$$

2.4. Overall Algorithm

Figure 4 illustrates the process of initialization of the coupling method, as well as the exchange of information between these solvers.

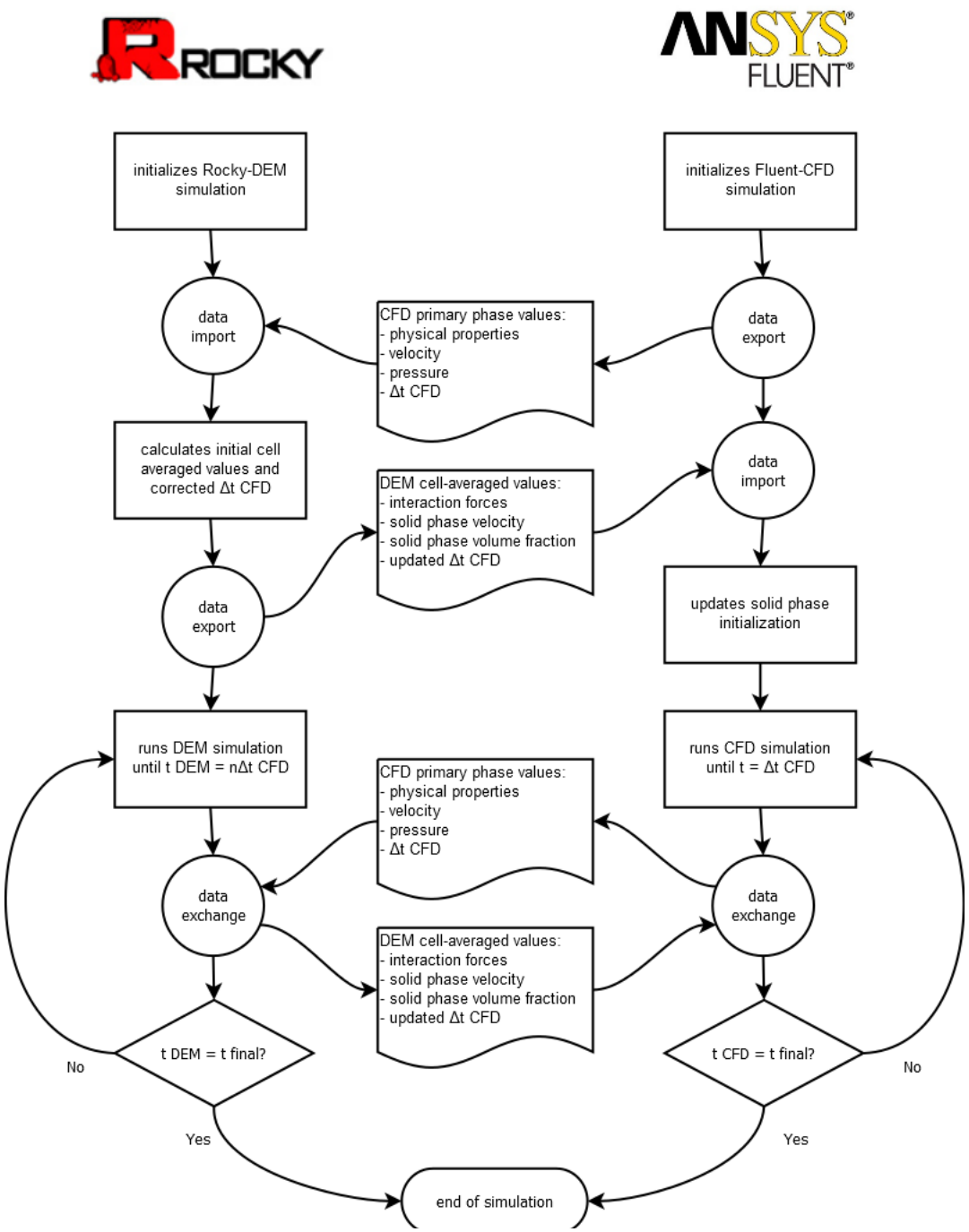

Figure 4: Schematic algorithm of the coupling numeric between Rocky® and Fluent®.

3. PROBLEM DESCRIPTION

3.1. Experimental Facility

Experimental data of SSCP-I were obtained in a 3 in x 9 in x 48 in bubbling fluidized bed with rectangular cross section, as illustrated in Figure 5(a). The bed material for the experiment was Geldart group D particles of uniform size and high sphericity. A low frequency (1 Hz) transducer was used to measure the mean pressure drop across two heights, as can be seen in Figure 5(b).

(a) **(b)**

Figure 5: (a) SSCP-I test facility and (b) Experimental facility showing pressure intakes

3.2. Geometry and Simulation Set-up

The experimental system was modeled by a column with rectangular cross-section. The gas distributor was not included in the domain, so that the gas enters the domain through the bottom with uniform superficial velocity, as shown in Figure 6(a). The gas leaves the domain through the top, which is under atmospheric conditions. A uniform grid with an initial bed composed by 92949 spherical particles with diameter of 3.256 mm and initial height of 16.4 cm was prescribed at the beginning of the simulation, as can be seen in Figure 6(b).

In order to monitor the particles and pressure drop response to increasing gas flow rate, the superficial velocity of the gas was linearly increased from 0 to the target final velocity during 2 s and kept at this value after that. The time step of the DEM simulations for the linear hysteresis normal force model is defined by material stiffness, mass of particles and number of time step per loading cycle. The time step for the CFD simulations was recalculated as the closest value that is a multiple of the DEM time step, based on an initial time step, as detailed in Figure 4. The geometry and simulation set-up details are gathered at Table 1.

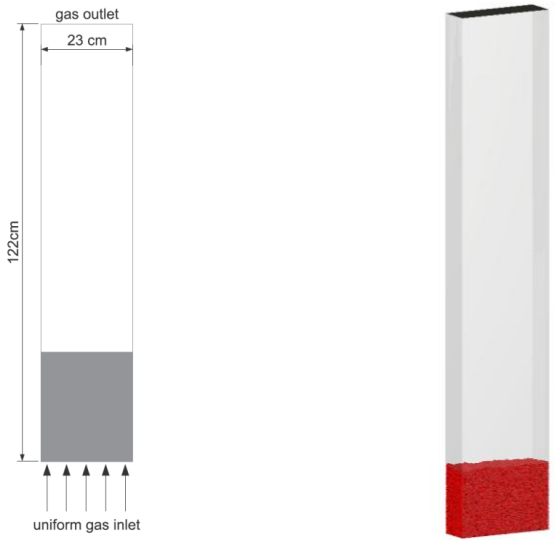

(a) **(b)**

Figure 6: (a) computational domain and fluid boundary conditions (b) initial particles bed

Table 1: Domain and simulation set-up.

		Value	Units
Domain	Domain size (W x D x H)	23 x 8 x 123	mm
	Grid cells	24 x 8 x 124	-
Particles	Particle diameter (d_p)	3.256	mm
	Particle density (ρ_p)	1131	kg m^{-3}
	Mass of inventory (M_p)	1.90	kg
	Particle-particle static and dynamic friction coefficients ($\mu_{s,p\text{-}p}$, $\mu_{d,p\text{-}p}$)	0.30	-
	Particle-wall static and dynamic friction coefficient ($\mu_{s,p\text{-}w}$, $\mu_{s,p\text{-}w}$)	0.35	-
	Particle-particle restitution coefficient ($\varepsilon_{p\text{-}p}$)	0.92	-
	Particle-wall restitution coefficient ($\varepsilon_{p\text{-}w}$)	0.84	-
	Particle Young's Modulus	10^7	N m^{-2}
	Wall Young's Modulus	10^{11}	N m^{-2}
Fluid	Gas density	1.20	kg m^{-3}
	Gas viscosity	1.90E-05	Pa s
	Gas inlet final velocity	2.18	m s^{-1}
	Time step (before correction)	10^{-3}	s

4. NUMERICAL RESULTS

The minimum fluidization velocity and the pressure drop across the bed are the most common values of interest in the design of such operations. The pressure drop on the flow of a fluid through a bed of particles can be estimated using, for example, the Ergun (1958) equation (Equation **(20)**). The minimum fluidization velocity, U_{MF}, can be estimated equating the pressure drop to the effective weight of the particles at the moment of incipient fluidization using the know Ergun's equation, as seen in Equation (21).

$$\frac{\Delta P}{H} = 150\frac{\left(1-\alpha_f\right)^2 \mu_f U}{\alpha_f^3 d_p^2 \phi^2} + 1.75\frac{\rho_f \left(1-\alpha_f\right) U^2}{\alpha_f^3 d_p \phi} \tag{20}$$

$$150\frac{\left(1-\alpha_f\right)^2 \mu_f U}{\alpha_f^3 d_p^2 \phi^2} + 1.75\frac{\rho_f \left(1-\alpha_f\right) U^2}{\alpha_f^3 d_p \phi} - g\left(1-\alpha_f\right)\left(\rho_p - \rho_f\right) = 0 \tag{21}$$

where H is the bed height and U is the fluid superficial velocity.

In order to evaluate the pressure drop behavior obtained at simulation, the predicted pressure drop by Ergun's correlation was calculated for 3 different fluid volume fraction values (α_f = 0.35, 0.4 and 0.45) for a range of fluid velocities. These curves are plotted as coloured dashed lines in the Figure 7. It is important to point out that these curves are valid until the fluidization starts, which is obtained at the point where the correlation minimum fluidization velocity curve (obtained by solving Equation (21) and shown by a black dashed line) crosses the pressure drop curve. The simulated pressure drop between the gas inlet and outlet is plotted in Figure 7 as a continuous orange line. The agreement between the pressure drop predicted by Ergun's correlation and the pressure drop obtained at simulation is fairly good until fluidization takes place.

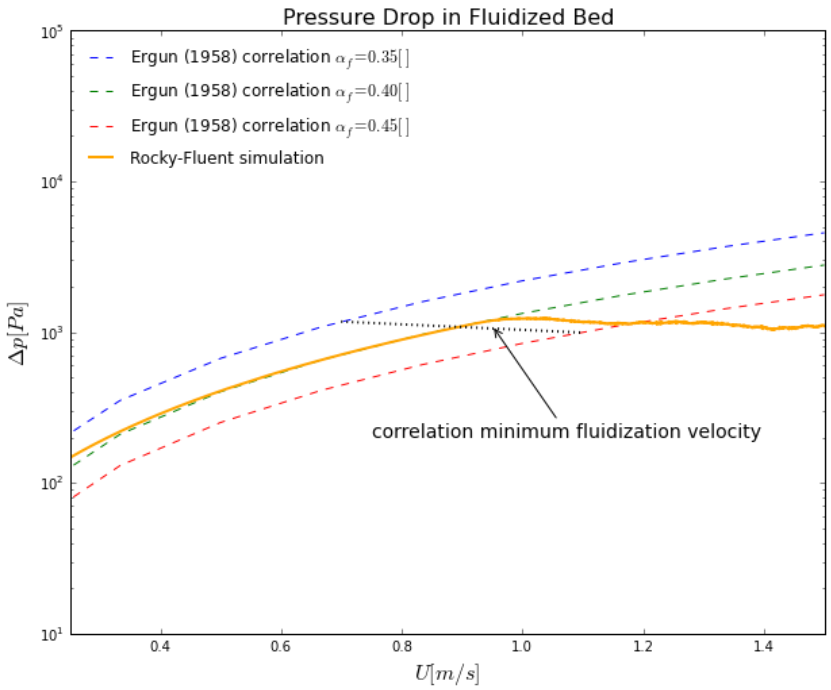

Figure 7: Pressure drop in fluidized bed case - comparison between simulation and correlation results.

The simulated pressure drop between the two pressure intake locations is shown in Figure 8 and compared to the averaged pressure drop value obtained experimentally. At the same plot, the red dashed line marks the moment at which the minimum fluidization velocity measured at experiments is achieved. It can be seen that it coincides well with the point at which the behavior of the pressure drop changes from linear to constant at simulation.

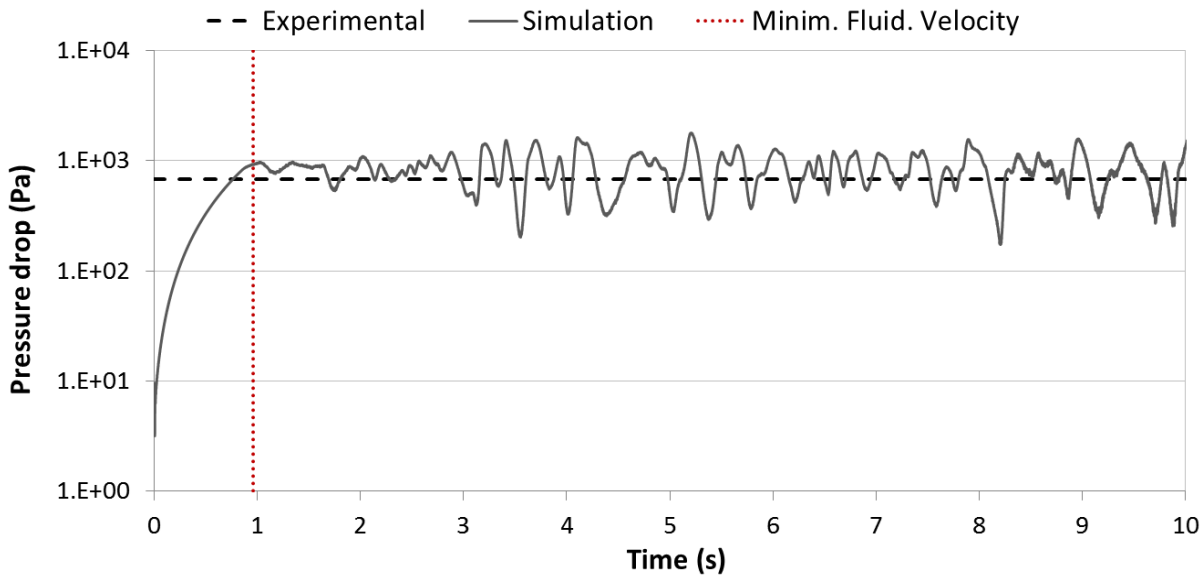

Figure 8: Evolution of pressure drop between the two pressure intake locations - comparison between simulation and experimental results.

In order to observe the behavior of the particles before and after fluidization starts, particles were divided into 7 different groups according to their initial position, as can be seen in Figure 9(a) and these particles groups were then tracked long time. Figure 9(b) shows the moment in which fluidization is about to start, and as expected, particles positions and bed height is nearly the same from initialization. Figure 9(c) shows the fluidization process with the gas superficial velocity gradually increase, while Figure 9(d) shows the particles location at the moment in which final velocity is achieved. Bubbles formation can observed beyond minimum fluidization velocity, confirming the expected bubbly regime, characteristic for fluidized beds operation. Lastly, Figure 9(f) displays the particles configuration after 5s of simulation, showing that particles are completely mixed, which confirms one of the main advantages of the used of the fluidized bed concept on nuclear reactors.

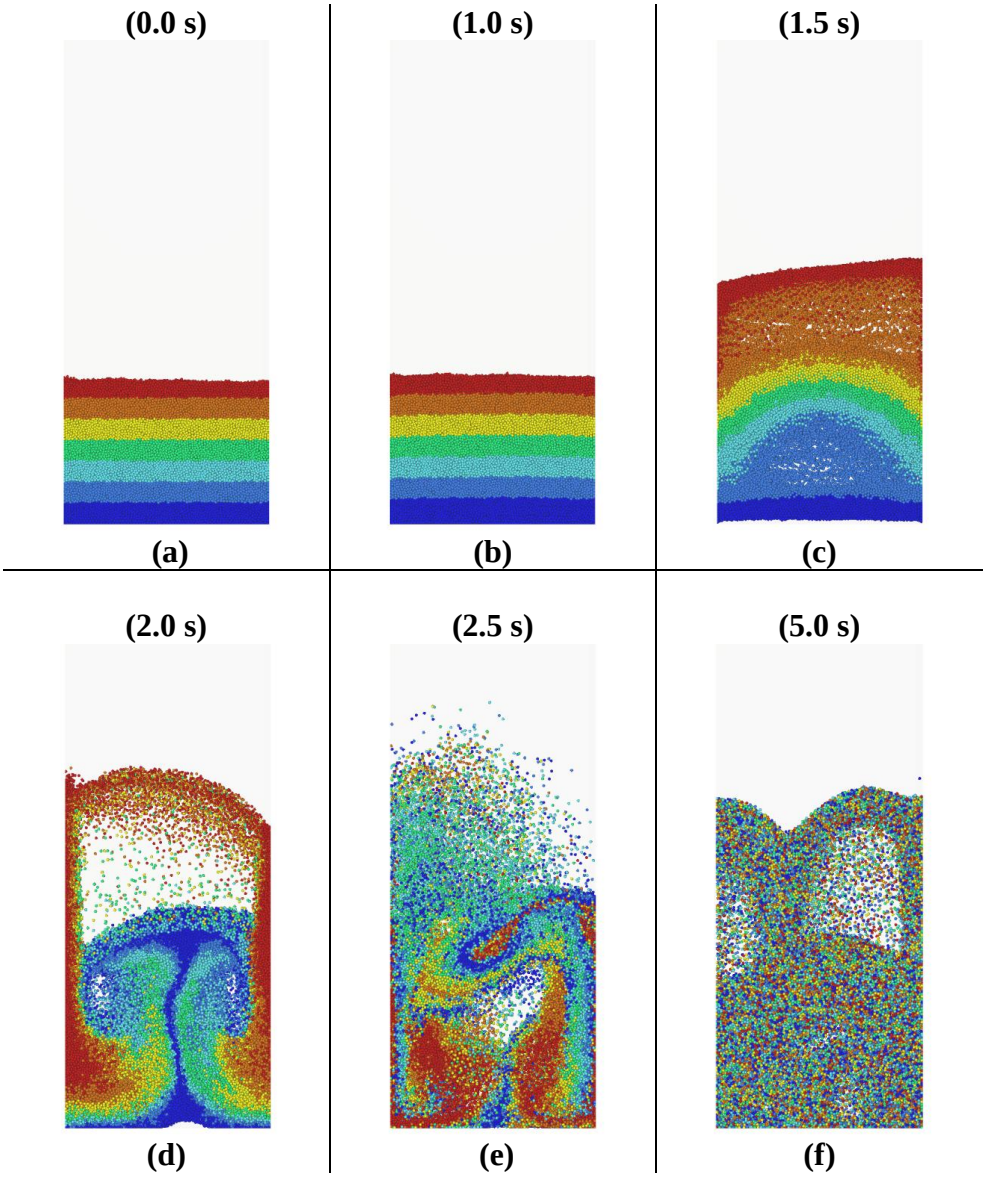

Figure 9: Evolution of particle behavior with time.

5. CONCLUSIONS

In this work, coupling between DEM and CFD packages Rocky® and ANSYS Fluent® was implemented and demonstrated through a numerical example. Mathematical modeling was presented, focusing on DEM, CFD and the coupling methods. The CFD-DEM coupling was applied to the simulation of a bubbling fluidized bed and the numerical results showed good agreement when compared to experimental data, confirming the proposed approach as a suitable alternative for modelling the fluid dynamics of fluidized bed nuclear reactors, providing detailed information of its behavior. Future developments for this coupling include implementation of thermal fluid-particle coupling between fluid and particles, enabling the evaluation of temperature distribution on a conceptual fluidized bed nuclear reactor.

6. ACKNOWLEDGEMENTS

The authors thank gratefully the financial support of CNPq, FAPERJ and CAPES during the realization of this work.

REFERENCES

[1] M. Scheve, "Liquid Fluidized Bed Reactor Program," *Proc. American Power Conf.*, Chicago, Illinois (1960).

[2] F. Sefidvash, "A fluidized bed nuclear reactor concept," *Nuclear Technology,* **71**, pp. 527-534 (1985).

[3] A. Agung, Conceptual design of a fluidized bed nuclear reactor, statics, dynamics and safety-related aspects, vol. PhD Thesis, Technische Universiteit Delft (2007).

[4] C. Pain, "An investigation of power stabilisation and space-dependent dynamics of a nuclear fluidized-bed reactor," *Nuclear Science and Engineering,* **144**, pp. 242-257 (2003).

[5] C. Pain, "A model of heat transfer dynamics of coupled multiphase-flow and neutron-radiation: application to a nuclear fluidized bed reactor," *International Journal of Numerical Methods for Heat and Fluid Flow,* **15**, pp. 765-807 (2005).

[6] F. Sefidvash, "Status of the small modular fluidized bed light water nuclear reactor concept," *Nuclear Engineering and Design,* **167**, pp. 203-214 (1996).

[7] F. Taghipour, N. Ellis e C. Wong, "Experimental and computational study of gas–solid fluidized bed hydrodynamics," *Chemical Engineering Science,* **60**, pp. 6857-6867 (2005).

[8] G. Liu, Y. Yang, H. Lu, E. You e X. Li, "Numerical Simulation of Particle Flow Motion in a Two-Dimensional Modular Pebble-Bed Reactor with Discrete Element Method," *Science and Technology of Nuclear Installations,* p.12 (2013).

[9] B. Hoomans, J. Kuipers, W. Briels e W. Van Swaaij, "Discrete particle simulation of bubble and slug formation in a two-dimensional gas-fluidized bed: a hard-sphere approach," *Chemical Engineering Science,* **60**, pp. 99-118 (1996).

[10] Y. Tsuji, T. Kawaguchi e T. Tanaka, "Discrete particle simulation of two dimensional fluidized bed," *Powder Technol,* **77**, pp. 79-87 (1993).

[11] B. Xu e A. Yu, "Numerical simulation of the gas–solid flow in a fluidized bed by combining discrete particle method with computational fluid dynamics," *Chemical Engineering Science,* **52**, pp. 2785-2809 (1997).

[12] D. Drew, "Mathematical modeling of two-phase flow," *Ann Rev Fluid Mech,* **15**, pp. 261-291 (1983).

[13] H. Zhu, Z. Zhou, R. Yang e A. Yu, "Discrete particle simulation of particulate systems: a review of major applications and findings," *Chemical Engineering Science,* **63**, pp. 5728-5770 (2008).

[14] "https://mfix.netl.doe.gov/challenge/index.php," (2013).

[15] O. Walton, "Numerical simulation of inelastic, frictional particle-particle interactions," *Particulate Two-Phase Flow*, Butterworth-Heinemann, M.C. Roco, pp. 884-911 (1993).

[16] O. Walton, "Force models for particle-dynamics simulations of granular materials," *NATO ASI Series E: Applied Sciences*, **287**, pp. 367-379 (1989).

[17] V. Vasquez e V. Ivanov, "A Phase Coupled Method for Solving Multiphase Problems on Unstructured Meshes," *Proceeding of ASME FEDSM'00: ASME 2000 Fluids Engineering Division Summer Meeting*, Boston, Massachusetts (2000).

[18] H. Ishii, Thermo-Fluid Dynamic Theory of Two-Phase Flow, Eyrolles, Paris (1975).

[19] S. Soo, Multiphase Fluid Dynamics, Science Press, Beijing (1990).

[20] D. Gidaspow, Multiphase Flow and Fluidization: Continuum and Kinetic Theory Descriptions, Academic Press, London (1994).

[21] P. Traoré, J. Laurentie e L. Dascalescu, "An efficient 4 way coupling CFD–DEM model for dense gas–solid particulate flows simulations," *Computers & Fluids,* **113**, pp. 65-76 (2015).

[22] B. Hutchinson e G. Raithby, "A Multigrid Method Based on the Additive Correction Strategy," *Numer. Heat Transfer,* **9**, pp. 511-537 (1986).

[23] C. Crowe, J. Schwarzkopf, M. Sommerfeld e Y. Tsuji, Multiphase Flows with Droplets and Particles, CRC Press, Boca Raton, Florida (2012).